

Theoretical analysis of the optical rotational Doppler effect under atmospheric turbulence by mode decomposition

Sheng-Jie Ma(马圣杰), Shi-Long Xu(徐世龙), Xiao Dong(董骁), Xin-Yuan Zhang(张鑫源),You-Long Chen(陈友龙), and Yi-Hua Hu(胡以华)

Citation: Chin. Phys. B, 2023, 32 (**10**): 104208. DOI: 10.1088/1674-1056/acc1d0
Journal homepage: http://cpb.iphy.ac.cn; http://iopscience.iop.org/cpb

What follows is a list of articles you may be interested in

Numerical simulation of super-continuum laser propagation in turbulent atmosphere

Ya-Qian Li(李雅倩), Wen-Yue Zhu (朱文越), and Xian-Mei Qian(钱仙妹)
Chin. Phys. B, 2021, 30 (**3**): 034201. DOI: 10.1088/1674-1056/abd38a

Non-Gaussian statistics of partially coherent light inatmospheric turbulence

Hao Ni(倪昊), Chunhao Liang(梁春豪), Fei Wang(王飞), Yahong Chen(陈亚红), Sergey A. Ponomarenko, Yangjian Cai(蔡阳健)
Chin. Phys. B, 2020, 29 (**6**): 064203. DOI: 10.1088/1674-1056/ab8373

Experimental demonstration of influence of underwater turbulence on ghost imaging

Man-Qian Yin(殷曼倩), Le Wang(王乐), Sheng-Mei Zhao(赵生妹)
Chin. Phys. B, 2019, 28 (**9**): 094201. DOI: 10.1088/1674-1056/ab33ee

Influence of moderate-to-strong anisotropic non-Kolmogorov turbulence on intensity fluctuations of a Gaussian-Schell model beam in marine atmosphere

Mingjian Cheng(程明建), Lixin Guo(郭立新), Jiangting Li(李江挺)
Chin. Phys. B, 2018, 27 (**5**): 054203. DOI: 10.1088/1674-1056/27/5/054203

Effect of atmospheric turbulence on entangled orbital angular momentum three-qubit state

Xiang Yan(闫香), Peng-Fei Zhang(张鹏飞), Jing-Hui Zhang(张京会), Xiao-Xing Feng(冯晓星), Chun-Hong Qiao(乔春红), Cheng-Yu Fan(范承玉)
Chin. Phys. B, 2017, 26 (**6**): 064202. DOI: 10.1088/1674-1056/26/6/064202

Theoretical analysis of the optical rotational Doppler effect under atmospheric turbulence by mode decomposition

Sheng-Jie Ma(马圣杰)[1,2], Shi-Long Xu(徐世龙)[1,2,†], Xiao Dong(董骁)[1,2], Xin-Yuan Zhang(张鑫源)[1,2], You-Long Chen(陈友龙)[1,2], and Yi-Hua Hu(胡以华)[1,2,‡]

[1] *State Key Laboratory of Pulsed Power Laser Technology, National University of Defense Technology, Hefei* 230037, *China*
[2] *Key Laboratory of Electronic Restriction of Anhui Province, National University of Defense Technology, Hefei* 230037, *China*

(Received 20 August 2022; revised manuscript received 2 February 2023; accepted manuscript online 7 March 2023)

The optical rotational Doppler effect associated with orbital angular momentum provides a new means for rotational velocity detection. In this paper, we investigate the influence of atmospheric turbulence on the rotational Doppler effect. First, we deduce the generalized formula of the rotational Doppler shift in atmospheric turbulence by mode decomposition. It is found that the rotational Doppler signal frequency spectrum will be broadened, and the bandwidth is related to the turbulence intensity. In addition, as the propagation distance increases, the bandwidth also increases. And when $C_n^2 \leq 5\times10^{-15}$ m$^{-2/3}$ and $2z \leq 2$ km, the rotational Doppler signal frequency spectrum width d and the spiral spectrum width d_0 satisfy the relationship $d = 2d_0 - 1$. Finally, we analyze the influence of mode crosstalk on the rotational Doppler effect, and the results show that it destroys the symmetrical distribution of the rotational Doppler spectrum about $2l\cdot\Omega/2\pi$. This theoretical model enables us to better understand the generation of the rotational Doppler frequency and may help us better analyze the influence of the complex atmospheric environment on the rotational Doppler frequency.

Keywords: optical rotational Doppler effect, atmospheric turbulence, vortex beam, mode decomposition, mode crosstalk

PACS: 42.68.Bz, 92.10.Lq, 42.79.Qx **DOI:** 10.1088/1674-1056/acc1d0

1. Introduction

The well-known Doppler frequency shift can be expressed as $\Delta f = 2vfc^{-1}$, which shows that when there is a linear relative motion between the source and the observer, a frequency shift will be generated, and this phenomenon is also called the linear Doppler effect (LDE). The frequency shift varies with the relative velocity between the source and the observer, and it is extensively used in Doppler velocity detection along the line of sight.[1,2] When a beam with a helical phase structure (such as a vortex beam) illuminates a rotating object with an optically rough surface, another type of Doppler frequency shift will occur, namely the rotational Doppler effect (RDE).[3–7] In 1992, Allen *et al.* discovered the vortex beam with a helical phase factor $\exp(\mathrm{i}l\varphi)$ carries orbital angular momentum (OAM),[8] where φ is the azimuthal angle, l is the topological charge (TC), and l is also called the OAM mode index. Since then, the vortex beam has been widely researched in optical communication,[9–11] optical manipulation,[12,13] and other fields. In recent years, vortex beams have also been widely used in rotational velocity detection, angular velocity detection, locating the center of rotating objects based on RDE.[5,6,14,15]

In 2013, Lavery *et al.* designed a rotational velocity measurement scheme based on RDE by collecting and analyzing the OAM beam scattered from a spinning object with an optically rough surface.[4] They discovered that the rotational Doppler frequency shift of a rotating object illuminated by an OAM-carrying beam can be expressed by $\Delta f = l\Omega/2\pi$, which showed that the frequency shift is only related to the rotational velocity of the spinning object and the OAM mode index. Since then, many kinds of research on rotational velocity detection based on RDE have been published.[16–18] Qiu *et al.* analyzed the RDE at the oblique light incidence and formulated the quantitative relation between the Doppler frequency shift and the tilt angle.[16] In the same year, they experimentally analyzed the influence of lateral misalignment on RDE. They concluded that the Doppler signal would be spectra-broadened when the beam axis of a probe light is not coincide with the rotation axis of the spinning object.[17] Based on this research, Zhang *et al.* analyzed the rotation velocity detection with orbital angular momentum light spot completely deviated from the rotation center.[18] However, most existing studies[14–18] are based on ideal conditions, and the influence of atmospheric disturbance on a vortex beam has not been considered. In Ref. [19], Zhang *et al.* established a 120 m long free-space link and experimentally analyzed the influence of atmospheric turbulence (AT) on the RDE. But they did not explain how AT affects the rotational Doppler frequency shift. In fact, especially for the free-space optical link, the propagation of vortex beams will be influenced by many factors, such as atmospheric turbulence, atmospheric scattering, aerosol, and so on. In this paper, we mainly analyze the influence of AT

†Corresponding author. E-mail: xushi1988@yeah.net
‡Corresponding author. E-mail: skl_hyh@163.com

© 2023 Chinese Physical Society and IOP Publishing Ltd

on vortex beams. The AT will lead to random variations in the refractive index, and the wavefront of the beam will be inevitably distorted, which will lead to a series of influences such as inter-symbol interference, signal power reduction, and so on.[20] The impact of AT on optical communication systems has been studied by many researchers.[21–23] However, the influence of AT on RDE has not been analyzed in the existing research, which is a non-ignorable part of RDE for practical applications.

In this paper, we theoretically analyze the influence of AT on RDE by mode decomposition and deduce the relationship between the rotational Doppler signal frequency spectrum and the AT intensity. Theoretical analysis shows that AT will lead to the expansion of the rotational Doppler signal frequency spectrum to adjacent modes. And when $C_n^2 \leq 5\times10^{-15}$ m$^{-2/3}$ and $2z \leq 2$ km, the rotational Doppler signal frequency spectrum width d and the spiral spectrum width d_0 satisfies the relationship of $d = 2d_0 - 1$. Finally, we analyze the influence of mode crosstalk on RDE, and the result indicates that mode crosstalk will lead to an asymmetric distribution of the rotational Doppler signal frequency spectrum. The research in this paper may help us better understand the mechanism of RDE and provide theoretical guidance for rotational object detection and OAM beam measurement.

2. Theoretical analysis

When a beam with a helical phase structure, such as the Laguerre–Gaussian (LG) beam, the Bessel beam, or the Airy–Gaussian beam, illuminates the surface of a rotating object, the rotational Doppler effect will occur.[16,24,25] Taking the LG beam as an example, the light field of the LG beam propagating along the z-axis can be expressed as

$$\begin{aligned} E_l^p(r,\varphi,z) = &\sqrt{\frac{2p!}{\pi(p+|l|)!}}\frac{1}{\omega(z)}\left[\frac{\sqrt{2}r}{\omega(z)}\right]^{|l|}\exp\left[\frac{-r^2}{\omega^2(z)}\right] \\ &\times L_p^{|l|}\left[\frac{2r^2}{\omega^2(z)}\right]\times\exp(-\mathrm{i}l\varphi)\exp\left[\frac{\mathrm{i}kr^2z}{2(z^2+z_\mathrm{R}^2)}\right] \\ &\times\exp\left[-\mathrm{i}(2p+|l|+1)\arctan(\frac{z}{z_\mathrm{R}})\right], \end{aligned} \tag{1}$$

where p and l are the radial index and topological charge, respectively, $L_p^{|l|}$ is the generalized Laguerre polynomial of the order p and degree $|l|$, $\omega(z) = \omega_0\sqrt{1+(z/z_\mathrm{R})^2}$ is the beam waist, $z_\mathrm{R} = \pi\omega_0^2/\lambda$ is the Rayleigh distance, and $k = 2\pi/\lambda$ is the wavenumber.

In Ref. [26], Fang *et al.* concluded that the RDE shared a common origin with LDE and the formula of rotational Doppler frequency shift could be derived from the linear Doppler frequency shift. The well-known linear Doppler frequency shift can be expressed as

$$\Delta f = \frac{2vf_0}{c}\cos\theta, \tag{2}$$

where f_0 is the frequency of the source light, v is the relative velocity between the source and the observer, and θ is the angle between the light propagation direction and the relative velocity vector direction. When $\theta = \pi/2$, i.e., the light propagation direction is perpendicular to the velocity vector direction, the linear Doppler shift equals 0 according to Eq. (2), which implies the LDE is not suitable to measure the spinning velocity. As for a vortex beam with a helical wavefront, there is an oblique angle between the Poynting vector and the beam propagation direction, which can be used for the application of RDE. As shown in Fig. 1(a), the angle between light propagation direction and Poynting vector can be expressed as $\sin\alpha = l\lambda/(2\pi r)$.[4] Under this circumstance, $\alpha+\theta = \pi/2$ and $\cos\theta = \sin\alpha = l\lambda/(2\pi r)$. Thus, Eq. (2) can be rewritten as

$$\Delta f = \frac{2vf_0}{c}\cos\theta = \frac{2vf_0}{c}\sin\alpha = \frac{2vf_0}{c}\frac{l\lambda}{2\pi r} = \frac{l\Omega}{2\pi}, \tag{3}$$

where Ω is the rotational velocity of the spinning object with an optically rough surface. Equation (3) shows the basic form of the rotational Doppler frequency shift. Unlike the LDE, the frequency shift based on RDE is only related to the rotational velocity Ω and the OAM mode index l. And it has nothing to do with the frequency of the source, which has been experimentally proved in Ref. [27]. In most existing experimental schemes, the light scattered from a spinning object with an optically rough surface is collected by a photodetector (PD), and the frequency shift spectrum can be obtained through real-time Fourier transform by an oscilloscope.[14–18] However, the accuracy of the experimental measurements depends on many factors. For example, when the power of the scattered light is too small, the PD may not receive any signal,[3,16] and when the reflectivity of the spinning object surface is not homogeneous, there will be both amplitude and phase modulation for the incident beam, which will reduce the Doppler shift.[28] As shown in Fig. 1(b), assuming that the OAM mode index of the vortex beam scattered from a spinning object is m, then the rotational Doppler frequency shift can be rewritten as

$$\Delta f = \frac{2vf_0}{c}(\sin\alpha - \sin\beta) = \frac{l-m}{2\pi}\Omega, \tag{4}$$

where β is the scattering angle. According to Eq. (4), when an OAM-carrying beam illuminates a spinning object with an optically rough surface, the frequency shift is related to the difference of the mode index between the incident and scattered beam and the rotating velocity.

On this basis, we add the influencing factor of AT. As is shown in Fig. 2(a), the vortex beam first propagates in the AT, and after being scattered by the rotating object, the scattered beam passes through AT again and finally received by the detector on the receiving end. Therefore, it is necessary to analyze the three processes of "propagation–scattering–propagation" of the vortex beam. Figure 2(b) shows the

equivalent model of two-way propagation. When the vortex beam passes through AT, its mode index will diffuse to adjacent modes and we assume that the mode index of OAM_l will expand to L, and then the mode indexes of the scattered vortex beam will be further diffused to L', and L' contains $\{l_1, l_2, \ldots, l_n\}$. Then, the rotational Doppler frequency shift can be expressed as

$$\Delta f = \frac{\sum_{i=1}^{n} l_i - m}{2\pi}\Omega. \tag{5}$$

The superimposed LG beam with two opposite TCs is widely used in RDE experiments. When propagating in AT, the mode index of the $\mathrm{OAM}_{l,-l}$ will expand to L' and $-L'$. Then the rotational Doppler frequency shift for the l part can be expressed as

$$\Delta f_L = \frac{\sum_{i=1}^{n} l_i - m}{2\pi}\Omega. \tag{6}$$

Similarly, the rotational Doppler frequency shift for the $-l$ part can be expressed as

$$\Delta f_{-L} = \frac{\sum_{j=1}^{n} l_j - m}{2\pi}\Omega, \tag{7}$$

where l_i is in L' and l_j is in $-L'$, representing the expanded mode indexes of the $\mathrm{OAM}_{l,-l}$ beam. Thus, the rotational Doppler frequency shift can be expressed as

$$\Delta f = \Delta f_L - \Delta f_{-L} = \frac{\sum_{i=1}^{n} l_i - \sum_{j=1}^{n} l_j}{2\pi}\Omega. \tag{8}$$

At this point, the frequency shift no longer has anything to do with the scattered beam mode index m, but only with the extended modes L', $-L'$, and the spinning velocity Ω. Compared with the single LG beam, the superimposed LG beam no longer needs to consider the scattered beam mode index, which also avoids the experimental errors caused by the inaccurate measurement of the scattered beam mode index m. When the rotating velocity Ω is a constant, the frequency shift is only related to the extended mode indexes, and how the OAM mode index will expand is related to AT intensity.

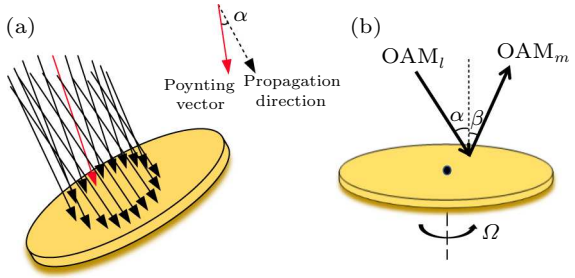


Fig. 1. (a) Schematic diagram of the incident OAM beam Poynting vector and object rotation axis. (b) Schematic diagram of the incident and scattered OAM beam mode index.

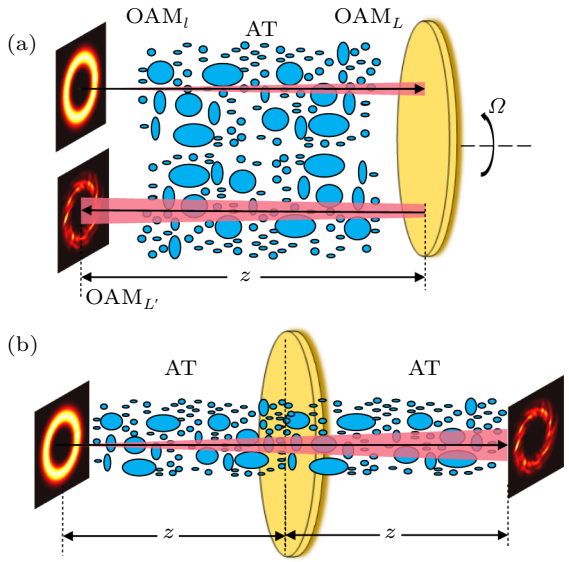


Fig. 2. (a) The two-way propagation model of vortex beam in AT. (b) The equivalent model of two-way transmission.

In the following, we will analyze the influence of AT on the OAM beam mode index by mode decomposition. The optical field $u(r,\theta,z)$ of the LG beam can be expanded by a helical spectrum function $\exp(\mathrm{i}m\theta)$ as[29]

$$u(r,\theta,z) = \frac{1}{\sqrt{2\pi}}\sum_{-\infty}^{\infty} a_m(r,z)\exp(\mathrm{i}m\theta), \tag{9}$$

where m is an integer number and $a_m(r,z)$ is the spiral spectrum coefficient, which can be expressed as

$$a_m(r,z) = \frac{1}{\sqrt{2\pi}}\int_0^{2\pi} u(r,\theta,z)\exp(-\mathrm{i}m\theta)\,\mathrm{d}\theta. \tag{10}$$

Then the square of modulus $a_m(r,z)$ can be expressed as

$$\begin{aligned}
&|a_m(r,z)|^2 \\
&= \frac{1}{2\pi}\int_0^{2\pi}\int_0^{2\pi} u(r,\theta_1,z)\exp(-\mathrm{i}m\theta_1)u^*(r,\theta_2,z) \\
&\quad\times\exp(-\mathrm{i}m\theta_2)\,\mathrm{d}\theta_1\,\mathrm{d}\theta_2 \\
&= \frac{1}{2\pi}\frac{1}{\omega^2(z)}\left[\frac{\sqrt{2}r}{\omega(z)}\right]^{2|m|}\left[L_p^{|l|}\left(\frac{2r^2}{\omega^2(z)}\right)\right]^2\exp\left(-\frac{2r^2}{\omega^2(z)}\right) \\
&\quad\times\int_0^{2\pi}\int_0^{2\pi}\langle\exp[\varphi(r,\theta_1,z)+\varphi^*(r,\theta_2,z)]\rangle \\
&\quad\times\exp[\mathrm{i}(l-m)\times(\theta_1-\theta_2)]\,\mathrm{d}\theta_1\,\mathrm{d}\theta_2.
\end{aligned} \tag{11}$$

For AT, $\langle\exp[\varphi(r,\theta_1,z)+\varphi^*(r,\theta_2,z)]\rangle$ can be expressed under the Rytov approximation as

$$\begin{aligned}
&\langle\exp[\varphi(r,\theta_1,z)+\varphi^*(r,\theta_2,z)]\rangle \\
&= \exp[\varphi(\boldsymbol{r}_1,z)+\varphi^*(\boldsymbol{r}_2,z)] \\
&= \exp\left[-\frac{1}{2}D_\varphi(\boldsymbol{r}_1-\boldsymbol{r}_2)\right] = \exp\left[\frac{(\boldsymbol{r}_1-\boldsymbol{r}_2)^2}{r_0^2}\right],
\end{aligned} \tag{12}$$

where $D_\varphi(\cdot)$ is the phase structure function, $\boldsymbol{r}_1, \boldsymbol{r}_2$ represent the vector directions of $(r,\theta_1),(r,\theta_2)$, respectively, $r_0 = (0.545C_n^2k^2z)^{-3/5}$ is the coherence length of AT, and C_n^2 is the

refractive index structure constant, which is usually used to measure the AT intensity.

To evaluate Eq. (11), we introduce the Bessel integral formula

$$\int_0^{2\pi} \exp\left[-\mathrm{i}n\theta_1 + \eta\cos(\theta_1-\theta_2)\right]\mathrm{d}\theta_1 = 2\pi\exp(-\mathrm{i}n\theta_1)I_n(\eta), \tag{13}$$

where $I_n(\cdot)$ is the modified Bessel function of integer order n. The energy content of different mode indexes can be obtained by radial integration of $|a_m(r,z)|^2$

$$\begin{aligned} C_m &= \int_0^R |a_m(r,z)|^2\,\mathrm{d}r \\ &= \frac{2\pi}{\omega^2(z)}\int_0^R \left[\frac{\sqrt{2}r}{\omega(z)}\right]^{2|m|}\left[L_p^{|l|}\left(\frac{2r^2}{\omega^2(z)}\right)\right]^2 \\ &\quad\times\exp\left(-\frac{2r^2}{\omega^2(z)}-\frac{2r^2}{r_0^2}\right)\times I_{m-l}\left(\frac{2r^2}{r_0^2}\right)r\,\mathrm{d}r, \end{aligned} \tag{14}$$

where R is the radius of the receiver aperture. Then the mth spiral spectrum components can be determined by the expression

$$P_m = C_m/\sum_{q=-\infty}^{\infty} C_q. \tag{15}$$

In the absence of AT, the OAM beam with the mode index l has the normalized power $P_m = 1$ for $m = l$ and $P_m = 0$ for $m \neq l$. In addition, the value of P_m remains unchanged with the increase of the propagation distance. When the OAM beam with mode index l propagates in AT, the value of P_m for $m = l$ will decrease and for $m \neq l$ will increase due to the random phase perturbations caused by AT. According to Eqs. (14) and (15), it is not difficult to find that mode index diffusion caused by AT has a symmetrical distribution about l, that is to say, the value of $P_{l+\Delta l}$ equals $P_{l-\Delta l}$. In this case, we can reasonably assume that the mode indexes of OAM$_l$ will expand to $\{l-2, l-1, l, l+1, l+2\}$ when propagating in AT. And the mode indexes of OAM$_{-l}$ will expand to $\{-l-2, -l-1, -l, -l+1, -l+2\}$ similarly. Under this circumstance, the rotational Doppler signal frequency shift will expand from $\{2l\}$ to $\{2l-4, 2l-3, 2l-2, 2l-1, 2l, 2l+1, 2l+2, 2l+3, 2l+4\}$ in $\Omega/2\pi$ units, and the power of each mode is determined by the corresponding energy weight according to Eq. (15).

According to the above theoretical analysis, we can conclude that the random phase perturbations caused by AT will lead to the expansion of the rotational Doppler signal frequency spectrum. The rotational Doppler signal frequency spectrum width d is dependent on the spiral spectrum width d_0 under the influence of AT, and the relationship between them can be expressed as $d = 2d_0 - 1$.

3. Simulation results and analysis

In Eq. (15), m can take the value of any integer, that is to say, the spiral spectrum can be expanded infinitely under the influence of AT. When P_m takes a very small value, we can consider there is no expansion anymore. In order to ensure the integrity of the spiral spectrum, we should first ensure a certain range of topological charges around l based on Eq. (14). Without loss of generality, we set the range of topological charges from $l-10$ to $l+10$ in this paper.

3.1. The influence of AT intensity on RDE

We first analyze the expansion of the spiral spectrum under different AT intensities. In the simulation, we set the initial parameters of the LG beam with $\lambda = 632.8$ nm, $\omega_0 = 0.01$ m, $l = 12$ and ± 12. Figures 3(a) and 3(b) show the beam intensity distribution and the spiral spectrum of the single LG beam with $l = 12$ and the superimposed LG beam with $l = \pm 12$ and the propagation distance is $2z = 1$ km. Without the influence of AT, the light intensity of the single LG beam with $l = 12$ presents a circular distribution, and the superimposed LG beam with $l = \pm 12$ has a petal-shaped intensity distribution, and the number of petals is $2l$. Under the influence of AT, the light intensity of the LG beam will be distorted, and the perfect ring-shaped light intensity structure begins to be deformed. As the intensity of AT increases, the dispersion of the light intensity also increases. When $C_n^2 = 1\times10^{-14}$ m$^{-2/3}$, the perfect ring-shaped light intensity structure is no longer visible. It is not difficult to find that the superimposed LG beam with $l = \pm 12$ will not affect the accuracy of the spiral spectrum, and the superimposed LG beam shows exactly the same spiral spectrum symmetrical about 0. When there is no AT, the spiral spectrum of the single LG beam with $l = 12$ is only distributed at $l = 12$, and the superimposed LG beam with $l = \pm 12$ shows a symmetrical distribution about 0 at $l = 12$ and $l = -12$. When $C_n^2 = 1\times10^{-16}$ m$^{-2/3}$, the spiral spectrum gradually expands to $l = \pm 11$ and ± 13. However, as the values of $P_{l=\pm11}$ and $P_{l=\pm13}$ are very small, we can ignore the expansion. With the increase of AT intensity, the spiral spectrum gradually expands to the adjacent modes. When $C_n^2 = 1\times10^{-15}$ m$^{-2/3}$, it expands to $l = \pm 11$ and $l = \pm 13$ and when $C_n^2 = 1\times10^{-14}$ m$^{-2/3}$, the spiral spectrum contains 18 modes $\{\pm8, \pm9, \pm10, \pm11, \pm12, \pm13, \pm14, \pm15, \pm16\}$. Meanwhile, the normalized power of $l = \pm 12$ decreases rapidly, and its value is less than 0.4. Under this circumstance, the expansion of the spiral spectrum is very serious.

The rotational Doppler signal frequency spectrum under different AT intensities is shown in Fig. 4. When $C_n^2 = 1\times10^{-15}$ m$^{-2/3}$, the spiral spectrum consists of six modes, including $\{\pm11, \pm12, \pm13\}$. According to Eq. (8), two modes of $l = 12$ and $l = -12$ will generate the frequency shift $\Delta f = 24\Omega/2\pi$ and $l = 12$ and $l = -13$ will

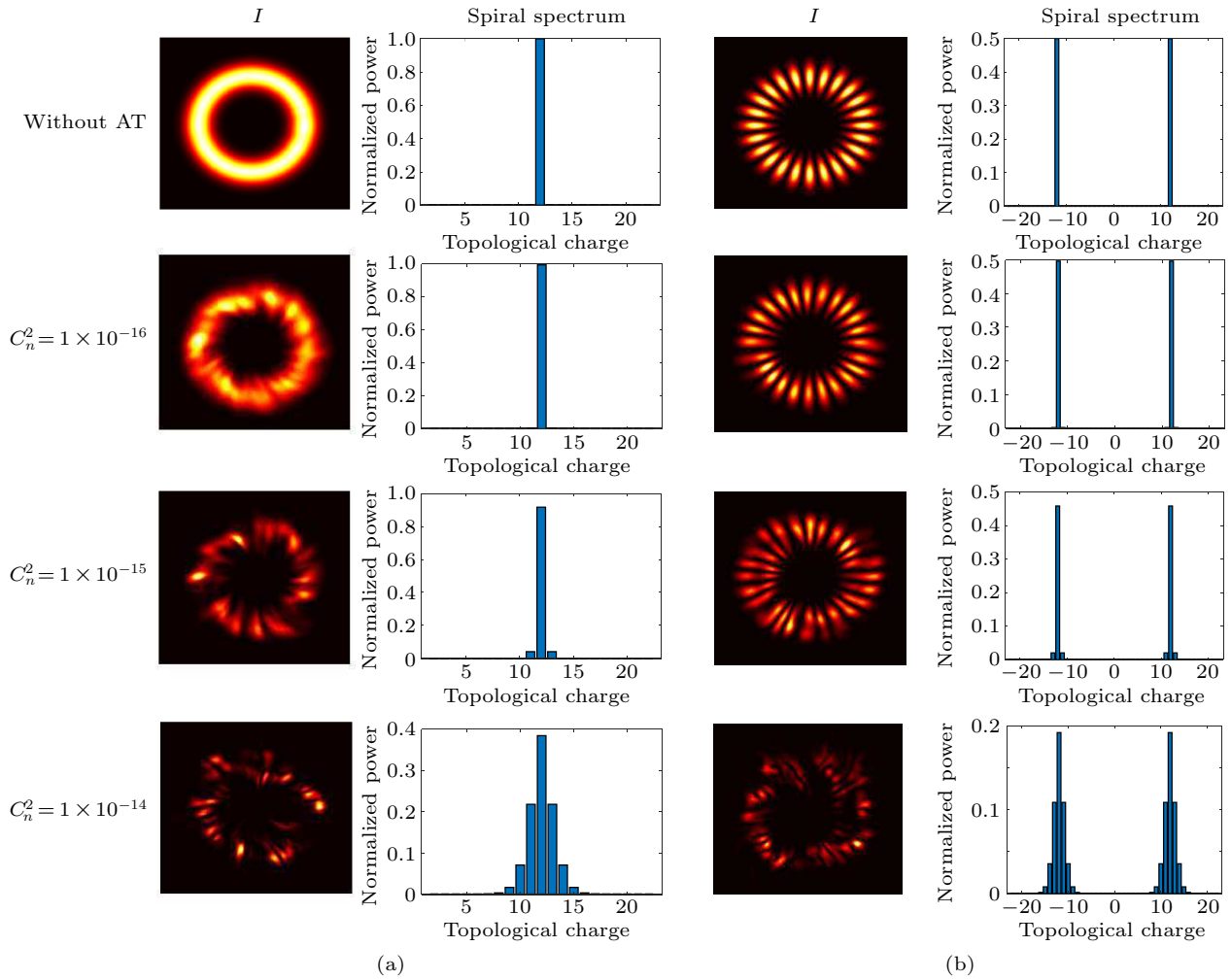


Fig. 3. Distribution of beam intensity and spiral spectrum under AT when propagation distance $2z = 1$ km. (a) The single LG beam with $l = 12$ and (b) the superimposed LG beam with $l = \pm 12$.

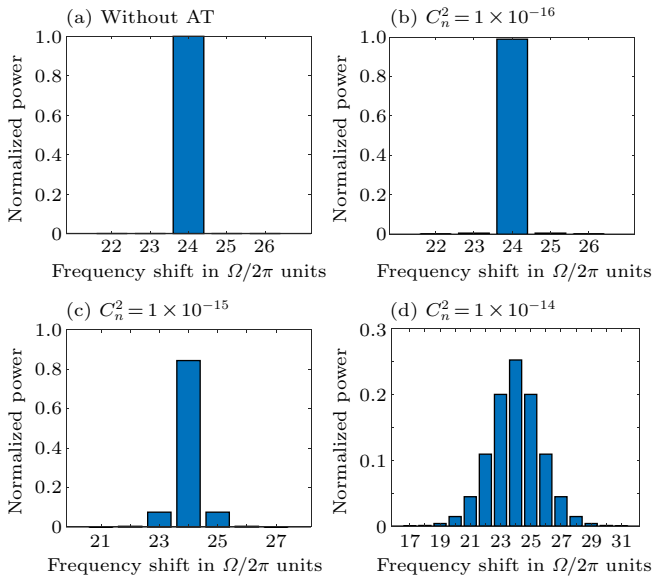


Fig. 4. Distribution of rotational Doppler signal frequency spectrum under different AT intensity.

generate the frequency shift $\Delta f = 25\Omega/2\pi$. Similarly, the rotational Doppler signal frequency spectrum will include $\{22,23,24,25,26\}$ in $\Omega/2\pi$ units. When $C_n^2 = 1\times10^{-14}$ m$^{-2/3}$, the spiral spectrum consists of 18 modes, including $\{\pm8,\pm9,\pm10,\pm11,\pm12,\pm13,\pm14,\pm15,\pm16\}$ and the Doppler signal frequency shift spectrum should theoretically contain 17 modes $\{16,17,\ldots,32\}$ in $\Omega/2\pi$ units. However, the width of the rotational Doppler signal frequency spectrum is less than the theoretical width in fact. As shown in Fig. 4(d), there are only 11 modes $\{19,20,\ldots,29\}$ in $\Omega/2\pi$ units. The reason may be that when spiral spectrum mode diffusion occurs, the modes adjacent to l have greater normalized power, and the normalized power of the remote modes will be further reduced or even be neglected in the calculation of the rotational Doppler frequency shift spectrum. Under this circumstance, the relationship between the rotational Doppler signal frequency spectrum width d and the spiral spectrum width d_0 no longer satisfies the relationship of $d = 2d_0 - 1$ but $d < 2d_0 - 1$.

The relationship curves of d and d_0 under different AT intensities are shown in Fig. 5. When $C_n^2 \le 5\times10^{-15}$ m$^{-2/3}$, the values of d_0 are 1, 1, 1, 3, and 5, and the corresponding values of d are 1, 1, 1, 5, and 9, respectively, and the values of d and d_0 satisfy the relationship $d = 2d_0 - 1$. When the value of

C_n^2 increases to 1×10^{-14} m$^{-2/3}$, $d=10$ and $d_0=9$ and they no longer satisfy the relationship $d=2d_0-1$ but $d<2d_0-1$. Therefore, we can conclude that when C_n^2 takes a small value, i.e., under weak AT, the spiral spectrum expansion caused by AT will lead to the expansion of the rotational Doppler signal frequency spectrum, and the rotational Doppler signal frequency spectrum width d satisfies the relationship $d=2d_0-1$. When C_n^2 takes a large value, the relationship between them changes to $d<2d_0-1$.

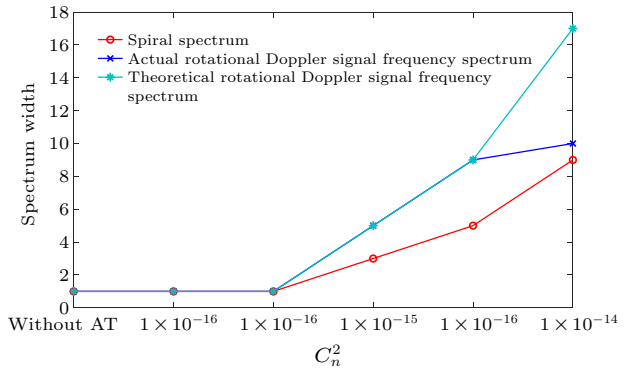


Fig. 5. Spectrum width of the spiral spectrum and rotational Doppler signal frequency spectrum under different AT intensities.

3.2. The influence of propagation distance on RDE

In addition, we set $C_n^2=1\times10^{-15}$ m$^{-2/3}$ as a fixed value to analyze the influence of the propagation distance $(2z)$ on the rotational Doppler signal frequency spectrum. Figure 6(a) shows the normalized power at $l=12$ of the single LG beam and $l=\pm12$ of the superimposed LG beam at different propagation distances. The normalized power of the single LG beam and the superimposed LG beam are 1 and 0.5 at the initial position, respectively. When the propagation distance increases to $2z=6$ km, the normalized power of the single LG beam and the superimposed LG beam reduces to 0.536 and 0.268, respectively. And under the same propagation distance, the normalized power of the superimposed LG beam is always half of the single LG beam, which is consistent with theoretical analysis. Figures 6(b) and 6(c) show the distribution of the spiral spectrum and the Doppler signal frequency spectrum under different propagation distances. When the propagation distance of the LG beam is less than $2z=2$ km, the spiral spectrum only spreads from $l=\pm12$ to $l=\pm11$ and ±13. And the corresponding rotational Doppler signal frequency spectrum includes 5 modes $\{22,23,24,25,26\}$ in $\Omega/2\pi$ units. When $2z=3$ km and 4 km, the spiral spectrum is further expanded to $\{\pm10,\pm11,\pm12,\pm13,\pm14\}$, and the rotational Doppler signal frequency spectrum contains 7 modes $\{21,22,23,24,25,26,27\}$ in $\Omega/2\pi$ units. When $z=6$ km, the spiral spectrum extends to 14 modes $\{\pm9,\pm10,\pm11,\pm12,\pm13,\pm14,\pm15\}$, and the corresponding rotational Doppler signal frequency spectrum also contains 9 modes $\{20,21,22,23,24,25,26,27,28\}$ in $\Omega/2\pi$ units.

According to the above analysis, when the AT intensity remains unchanged, the increase of propagation distance will also lead to rotational Doppler signal frequency spectrum expansion. It is not difficult to find that in the case of a short distance propagation ($2z<2$ km), the rotational Doppler signal frequency spectrum width d and the spiral spectrum width d_0 also satisfy the relationship $d=2d_0-1$, and $d<2d_0-1$ in the case of a long distance propagation.

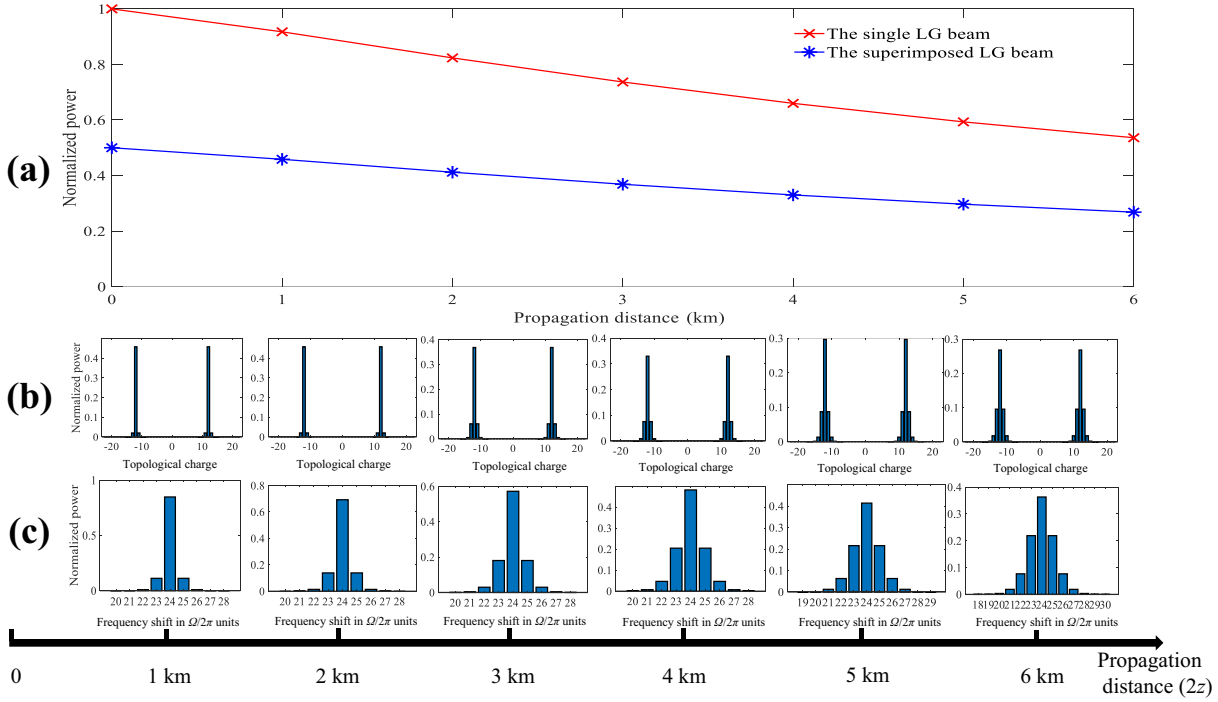


Fig. 6. (a) The normalized power at $l=12$ of the single LG beam with and $l=\pm12$ of the superimposed LG beam under different propagation distances; (b) and (c) are the spiral spectrum and rotational Doppler signal frequency spectrum, respectively.

3.3. The influence of mode crosstalk on RDE

In the above analysis, we set the value of TC to $l = 12$ of the single LG beam and $l = \pm 12$ of the superimposed LG beam. The reason why we choose a large value of TC is to avoid the crosstalk between different mode indexes caused by AT.[30] The crosstalk will ultimately lead to an increased bit error in the receiving end and a decreased capacity for the optical communication system.[31] Finally, we will analyze the influence of mode crosstalk on RDE. According to the spiral spectrum in Fig. 3(b), even when $C_n^2 = 1 \times 10^{-14}$ m$^{-2/3}$, we can still clearly see two peaks of the superimposed LG beam at $l = 12$ and $l = -12$. The minimum diffusion mode of $l = 12$ is $l = 8$, and the maximum diffusion mode of $l = -12$ is $l = -8$, so there is no intersection in the spiral spectrum, and the rotational Doppler signal frequency spectrum also presents one peak spectrum at $2l$ in $\Omega/2\pi$ units. If the TC of the superimposed LG beam takes a small value, crosstalk between different modes is likely to occur. Figure 7(a) shows the spiral spectrum with different values of l and C_n^2. In order to better verify this conjecture, we let C_n^2 take some large values: 5×10^{-15},

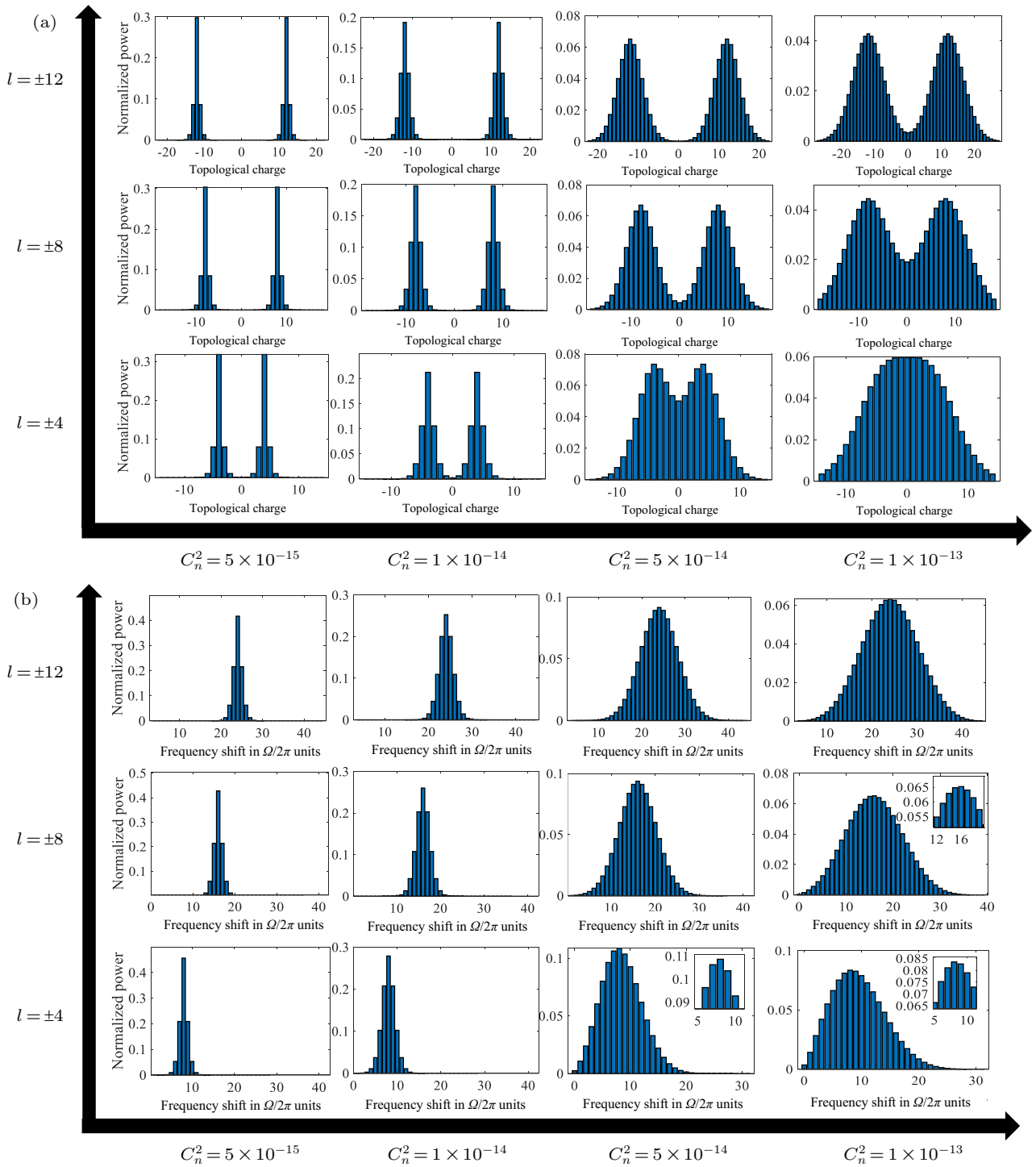


Fig. 7. (a) Spiral spectrum with different mode indexes and AT intensities. (b) Rotational Doppler signal frequency spectrum corresponding to panel (a).

Table 1. Normalized power of different modes with and without crosstalk.

		Normalized power of different modes in $\Omega/2\pi$ units						
		$2l-3$	$2l-2$	$2l-1$	$2l$	$2l+1$	$2l+2$	$2l+3$
Without crosstalk	$C_n^2=1\times10^{-14}$ m$^{-2/3}$, $l=\pm4$	0.037	0.102	0.201	0.279	0.201	0.102	0.037
	$C_n^2=1\times10^{-14}$ m$^{-2/3}$, $l=\pm8$	0.013	0.042	0.107	0.203	0.107	0.042	0.013
	$C_n^2=1\times10^{-14}$ m$^{-2/3}$, $l=\pm12$	0.045	0.110	0.200	0.253	0.200	0.110	0.045
With crosstalk	$C_n^2=5\times10^{-14}$ m$^{-2/3}$, $l=\pm4$	0.080	0.100	0.107	0.109	0.104	0.093	0.078
	$C_n^2=1\times10^{-13}$ m$^{-2/3}$, $l=\pm4$	0.056	0.067	0.076	0.084	0.083	0.079	0.073
	$C_n^2=1\times10^{-13}$ m$^{-2/3}$, $l=\pm8$	0.060	0.063	0.065	0.065	0.064	0.061	0.057

1×10^{-14}, 5×10^{-14}, 1×10^{-13} m$^{-2/3}$. For $l=\pm12$, mode crosstalk only occurs when $C_n^2=1\times10^{-13}$ m$^{-2/3}$. However, the mode crosstalk does not have a significant influence on the rotational Doppler signal frequency spectrum, and the two peak spectrums at $l=12$ and $l=-12$ can still be clearly identified. For $l=\pm8$, mode crosstalk begins to appear when $C_n^2=5\times10^{-14}$ m$^{-2/3}$ and the normalized power at $l=0$ is close to half of the maximum value when $C_n^2=1\times10^{-13}$ m$^{-2/3}$, which has a certain influence on the whole signal spiral spectrum. For $l=\pm4$, when $C_n^2=5\times10^{-14}$ m$^{-2/3}$, the normalized power at $l=0$ is 0.05, which is close to the normalized peak power. When $C_n^2=1\times10^{-13}$ m$^{-2/3}$, the normalized power at $l=0$ is already bigger than that at $l=\pm4$. What is worse, the original two peaks spectrum degenerated into one peak spectrum at $l=0$. At this time, the crosstalk between different modes was very serious, and the value of l could not even be intuitively determined by the spiral spectrum. According to the above analysis, mode crosstalk may change the structure of the spiral spectrum of the superimposed LG beam with $\pm l$, especially for l with a small value, and the normalized power adjacent to $l=0$ will increase, which will even cause the original two peaks spectrum to degenerate into a one peak spectrum.

The corresponding rotational Doppler signal frequency spectra are shown in Fig. 7(b). When there is no mode crosstalk, the rotational Doppler signal frequency spectrum is symmetrically distributed about $2l$ in $\Omega/2\pi$ units. And when mode crosstalk occurs, the symmetrical distribution of the rotational Doppler signal frequency spectrum about $2l$ in $\Omega/2\pi$ units is destroyed. Table 1 shows the normalized power of six modes adjacent to $2l$ in $\Omega/2\pi$ units under different conditions. When there is no crosstalk, the normalized power of $2l-1$ is the same as $2l+1$ in $\Omega/2\pi$ units and the rotational Doppler signal frequency spectrum is still symmetrically distributed about $2l$ in $\Omega/2\pi$ units. When $C_n^2=1\times10^{-14}$ m$^{-2/3}$, $l=\pm4$, crosstalk occurs, and the normalized powers of $\{2l-1,2l-2,2l-3\}$ in $\Omega/2\pi$ units are 0.107,0.100,0.080 and the normalized powers of $\{2l+1,2l+2,2l+3\}$ in $\Omega/2\pi$ units are 0.104,0.093,0.078, respectively. On this occasion, they are no longer symmetrically distributed about $2l$ in $\Omega/2\pi$ units. And the same phenomenon also occurs when $C_n^2=1\times10^{-13}$ m$^{-2/3}$, $l=\pm4$ and $C_n^2=1\times10^{-13}$ m$^{-2/3}$, $l=\pm8$. The reason for this may be that when mode crosstalk occurs, the normalized power of the modes adjacent to $l=0$ is increased, and the spiral spectrum is no longer symmetric about $\pm l$. Consequently, the rotational Doppler signal frequency spectrum shows an asymmetric distribution about $2l$ in $\Omega/2\pi$ units.

4. Conclusion and perspectives

In conclusion, we theoretically investigate the influence of AT on the rotational Doppler effect by modal expansion and deduce the formula of rotational Doppler frequency shift under the influence of AT. We find that AT will lead to the expansion of the rotational Doppler signal frequency shift spectrum from $2l$ in $\Omega/2\pi$ units to adjacent modes, and the diffusion will increase as the AT intensity and propagation distance increase. Moreover, under strong turbulence, mode crosstalk of different modes will occur, which will lead to an asymmetric distribution of the rotational Doppler signal frequency spectrum. Our theoretical analysis provides a new supplement for RDE and may promote the development of atmospheric detection for practical applications.

Acknowledgments

Project supported by the Research Plan Project of the National University of Defense Technology (Grant No. ZK18-01-02), the National Natural Science Foundation of China (Grant No. 61871389), the State Key Laboratory of Pulsed Power Laser Technology (Grant No. KY21C604), and the Postgraduate Scientific Research Innovation Project of Hunan Province (Grant Nos. CX20220007 and CX20230024).

References

[1] Truax B E, Demarest F C and Sommargren G E 1984 *Appl. Opt.* **23** 67
[2] Seddon N and Bearpark T 2003 *Science* **302** 1537
[3] Ding Y, Ren Y, Liu T, Qiu S, Wang C, Li Z and Liu Z 2021 *Opt. Express* **29** 15288
[4] Lavery M P J, Speirits F C, Barnett S M and Padgett M J 2013 *Science* **341** 537
[5] Qiu S, Ren Y, Liu T, Li Z, Liu Z, Wang C, Ding Y and Sha Q 2021 *Opt. Express* **29** 10275
[6] Zhai Y, Fu S, Zhang J, Lv Y, Zhou H and Gao C 2020 *Appl. Phys. Express* **13** 022012
[7] Ding Y, Ren Y, Liu T, Qiu S, Wang C, Li Z and Liu Z 2021 *Opt. Express* **29** 15288
[8] Allen L, Beijersbergen M W, Spreeuw R J C and Woerdman J P 1992 *Phys. Rev. A* **45** 8185

[9] Huang H, Xie G, Yan Y, Ahmed N, Ren Y, Yue Y, Rogawski D, Willner M J, Erkmen B I, Birnbaum K M, Dolinar S J, Lavery M P J, Padgett M J, Tur M and Willner A E 2014 *Opt. Lett.* **39** 197

[10] Ren Y, Wang Z, Liao P, Li L, Xie G, Huang H, Zhao Z, Yan Y, Ahmed N, Willner A, Lavery M P J, Ashrafi N, Ashrafi S, Bock R, Tur M, Djordjevic I B, Neifeld M A and Willner A E 2016 *Opt. Lett.* **41** 622

[11] Li L, Zhang R, Liao P, Cao Y, Song H, Zhao Y, Du J, Zhao Z, Liu C, Pang K, Song H, Almaiman A, Starodubov D, Lynn B, Bock R, Tur M, Molisch A F and Willner A E 2019 *Opt. Lett.* **44** 5181

[12] Grier D G 2003 *Nature* **424** 810

[13] Zhang Y, Shi W, Shen Z, Man Z, Min C, Shen J, Zhu S, Urbach H P and Yuan X 2015 *Sci. Rep.* **5** 15446

[14] Zhai Y, Fu S, Yin C, Zhou H and Gao C 2019 *Opt. Express* **27** 15518

[15] Ding Y, Liu T, Qiu S, Liu Z, Sha Q and Ren Y 2022 *Appl. Opt.* **61** 3919

[16] Qiu S, Liu T, Ren Y, Li Z, Wang C and Shao Q 2019 *Opt. Express* **27** 24781

[17] Qiu S, Liu T, Li Z, Wang C, Ren Y, Shao Q and Xing C 2019 *Appl. Opt.* **58** 2650

[18] Zhang Z, Cen L, Zhang J, Hu J, Wang F and Zhao Y 2020 *Opt. Express* **28** 6859

[19] Zhang W, Gao J, Zhang D, He Y, Xu T, Fickler R and Chen L 2018 *Phys. Rev. Appl.* **10** 044014

[20] Paterson C 2005 *Phy. Rev. Lett.* **94** 153901

[21] Li S, Chen S, Gao C, Willner A E and Wang J 2018 *Opt. Commun.* **408** 68

[22] Zheng D, Li Y, Zhou H, Bian Y, Yang C, Li W, Qiu J, Guo H, Hong X, Zuo Y, Giles I P, Tong W and Wu J 2018 *Opt. Express* **26** 28879

[23] Wang Y, Xu H, Li D, Wang R, Jin C, Yin X, Gao S, Mu Q, Xuan L and Cao Z 2018 *Sci. Rep.* **8** 1124

[24] Qiu S, Ren Y, Sha Q, Ding Y, Wang C, Li Z and Liu T 2021 *Opt. Commun.* **490** 126900

[25] Fu S, Wang T, Zhang Z, Zhai Y and Gao C 2017 *Opt. Express* **25** 20098

[26] Fang L, Padgett M J and Wang J 2017 *Laser Photonics Rev.* **11** 1700183

[27] Lavery M P J, Barnett S M, Speirits F C and Padgett M J 2014 *Optica* **1** 1

[28] Zhou H, Fu D, Dong J, Zhang P and Zhang X 2016 *Opt. Express* **24** 10050

[29] Zeng J, Liu X, Zhao C, Wang F, Gbur G and Cai Y 2019 *Opt. Express* **27** 25342

[30] Zhang L, Shen F, Lan B and Tang A 2020 *Journal of Optics* **22** 075607

[31] Lv H, Ren C and Liu X 2020 *Infrared Phys. Technol.* **105** 103181